Growth-mode induced defects in epitaxial $SrTiO_3$ thin films grown on single crystal $LaAlO_3$ by a two-step PLD process

Dong Su[a)]
Ceramics Laboratory, Swiss Federal Institute of Technology, Lausanne CH-1015, Switzerland; and Department of Physics, Arizona State University, Tempe, Arizona 85287-1504

Tomoaki Yamada,[b)] Roman Gysel, Alexander K. Tagantsev, Paul Muralt,[c)] and Nava Setter
Ceramics Laboratory, Swiss Federal Institute of Technology, Lausanne CH-1015, Switzerland

Nan Jiang[d)]
Department of Physics, Arizona State University, Tempe, Arizona 85287-1504

(Received 6 September 2010; accepted 22 November 2010)

We grew epitaxial $SrTiO_3$ (STO) thin films on (001) $LaAlO_3$ substrates via a two-step procedure using pulsed laser deposition and studied them with transmission electron microscopy in plane-view and cross-sectional samples. We found that partial misfit dislocations are the main interfacial defects, whereas planar defects are the main defects in STO films. Our results suggest that a three-dimensional island mode dominates the growth of the STO film.

I. INTRODUCTION

The large tunability of permittivity and the relatively low dielectric loss at microwave frequency of $SrTiO_3$ (STO) and (Ba, Sr)TiO_3 thin films have fostered great interest in their applications in microwave-tunable devices.[1–3] However, experimental and theoretical studies demonstrated that strains, induced by lattice mismatch between these ferroelectric films and their substrates, strongly affect their dielectric properties. To resolve this, different relaxation techniques were assessed, such as using different substrates, post-annealing, adding interface layers, applying oxygen partial pressure, and changing film thickness.[4–7]

Earlier, we proposed a two-step growth method to mitigate strains in STO thin film, starting growth in the first step at a lower temperature to obtain a high nucleation density, followed by second-step growth at high temperature. We demonstrated an effective reduction in strain in epitaxial STO thin films on a $LaAlO_3$ (LAO) substrate using pulsed laser deposition (PLD).[8,9] We found that a 10-nm first layer (FL) can almost completely relax the strain induced by lattice mismatch between the film and its substrate. The two-step-grown STO film exhibited substantially higher permittivity and tunability than the conventional films grown by a single-step process, which were under compressive strain. We interpreted these dielectric responses of both types of film by Landau's theory, taking account of the difference in the residual strain in them.[10] To further understand the mechanism whereby the two-step growth process induces substantial strain relaxation, we undertook a comprehensive study on the microstructure of the STO film, as reported herein.

Generally, there are three typical modes of growth[11]: (i) two-dimensional (2D) layer-by-layer growth (the Frank der Merwe mode.); (ii) three-dimensional (3D) island growth (the Volmer–Weber mode); and (iii) the 2D–3D island-on-layer growth [the Stranski–Krastanov (SK) mode]. For single-step STO thin films grown by PLD under our experimental conditions, seemingly growth follows the SK mode, as indicated by the existence of dislocations and the enhanced surface roughness. In contrast, for films generated via two-step growth, the amorphous-FL is being crystallized after a few nanometers' growth, signifying that its growth would not be in accord with the SK mode. Therefore, it is interesting to consider how this change in the pattern of growth might affect the defects in the film.

In this work, we perform a detailed transmission electron microscopic (TEM) investigation on the microstructures of two-step-grown STO films on (001) LAO single crystals. We found that the defects in such films differ from those in conventionally single-step-grown film. We studied the surface morphology of the FL by atomic force microscope (AFM). On the basis of our experimental results, we proposed a growth mode to interpret the high

[a)]Present address: Center for Functional Nanomaterials, Brookhaven National Laboratory, Upton, New York 11973.
[b)]Present address: Department of Innovative and Engineered Materials, Tokyo Institute of Technology, 4259-J2-43, Nagatsuta-cho, Midori-ku, Yokohama 226-8502, Japan.
[c)]This author was an editor of this journal during the review and decision stage. For *JMR* policy on review and publication of manuscripts authored by editors, please refer to http://www.mrs.org/jmr_policy
[d)]Address all correspondence to this author.
e-mail: nan.jiang@asu.edu
DOI: 10.1557/jmr.2010.82

 © Materials Research Society 2011

https://doi.org/10.1557/jmr.2010.82 Published online by Cambridge University Press

intensity of planar defects in the two-step-grown films and discuss their effects on the dielectric properties of the film.

II. EXPERIMENTAL

As shown in Fig. 1 of Ref. 9, the two-step growth technique was used to deposit STO thin films on (001) LAO single-crystal substrates by PLD with KrF excimer laser ($\lambda = 248$ nm). The laser energy and the repetition rate were 220 mJ and 5 Hz, respectively. For the first stage of growth, we deposited a 10-nm-thick STO layer at 100 °C as a buffer layer. Then, we annealed the sample at 750 °C for 20 min to induce epitaxial crystallization. Finally, an STO film was deposited on the crystallized buffer layer at 750 °C to a depth of 250 nm. Reflection high-energy electron diffraction and x-ray diffraction showed that the epitaxial growth of conventionally grown films and those yielded from two-step growth have orientation relationship of (001)[100]STO//(001)[100]LAO (Here, we neglect the slight rhombohedral distortion of LAO and treat its structure as cubic. The [001] zone axis is normal to the interface.) The surface morphology of the films was studied using a thermo-microscope AFM operating in the contact mode. AFM cantilevers with a force constant of 3 nm were used. We prepared wedge-shaped cross-sectional and plane-view TEM specimens using triple polishing and followed by Ar-ion milling at 3 kV. Our observations were obtained via a CM20 TEM and a CM-300 FEG microscope (Philips Electron Optics, now FEI).

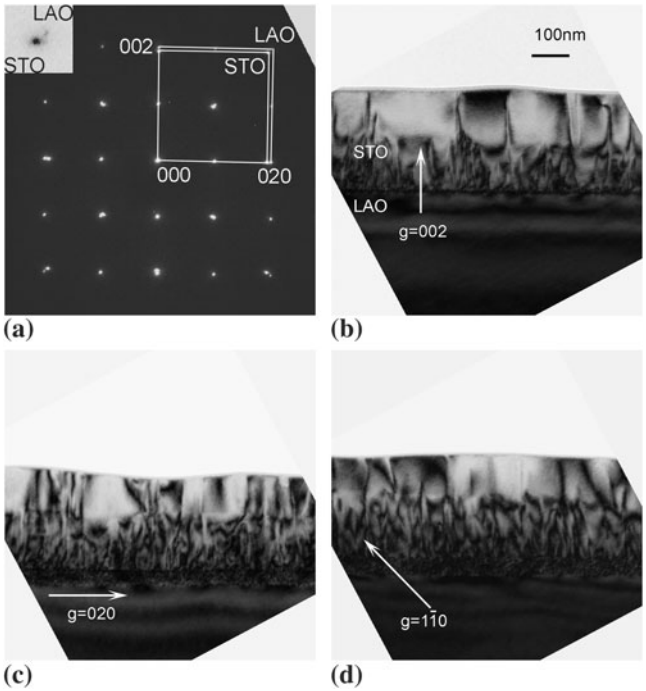


FIG. 1. (a) Selected area electron diffraction pattern on the cross-sectional $SrTiO_3$ (STO)/$LaAlO_3$ (LAO) [100] interface. (b)–(d) Bright field cross-sectional images on the interface between the two-step STO thin film and the LAO substrate. The first STO layer is 10-nm thick. The images were taken using (b) $\boldsymbol{g} = 002$, (c) $\boldsymbol{g} = 020$, and (d) $\boldsymbol{g} = 1\bar{1}0$.

III. RESULTS AND DISCUSSION

We characterized a cross-sectional sample along the [100] direction. Figure 1(a) illustrates the selected-area electron diffraction (SAED) pattern obtained from the interface between STO and LAO; it confirms that the crystallographic relationship is (001)[100]STO//(001)[100] LAO. Figures 1(b)–1(d) are bright-field (BF) images under two beam conditions with $\boldsymbol{g} = 002$, $\boldsymbol{g} = 020$, and $\boldsymbol{g} = 1\bar{1}0$. The contrast in the STO films can be either threading dislocations or planar defects. In the BF image of a conventional single-step-grown film, similar contrast was noted owing to threading dislocations using $\boldsymbol{g} = 020$ while it was not evident in an image using $\boldsymbol{g} = 002$.[12,13] On the contrary, here we observed the defects using both the 020 and 200 vectors, which points to the defects other than the threading dislocations. We identified them as stacking faults from high-resolution images and plane-view images, as discussed later in the text. We noted a higher density of defects in the film's lower part than in its upper part; evidently, strain was relaxed there, consistent with our previous reports.[8,9] In addition, in Figs. 1(c) and 1(d), we observed moiré fringes at the interface because of the overlapping of film and substrate.

Figure 2 is a high-magnification image along the [100] zone axis. Both perfect and partial dislocations are observed at the interface; furthermore, there is an interfacial stacking fault between the partial dislocations. The relative shift in the stacking fault is $1/2\boldsymbol{a}[011]$, consistent with an atomic shift from the oxygen atom to the neighboring strontium atom. The interfacial stacking fault might reflect the dissociation of perfect misfit dislocations during growth, as observed by others previously.[13,14] Above the partial dislocations, two other stacking faults extend into the STO film. In the two-step-grown thin films, we have observed a high density of the partial dislocation and

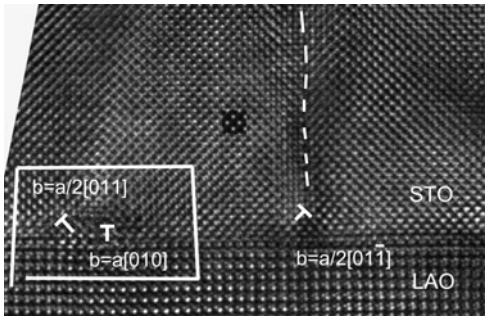


FIG. 2. A cross-sectional high-resolution image on the STO/LAO interface along the [100] zone axis. Partial and perfect dislocations are marked. The stacking fault in the STO film is denoted by a dashed line.

https://doi.org/10.1557/jmr.2010.82 Published online by Cambridge University Press

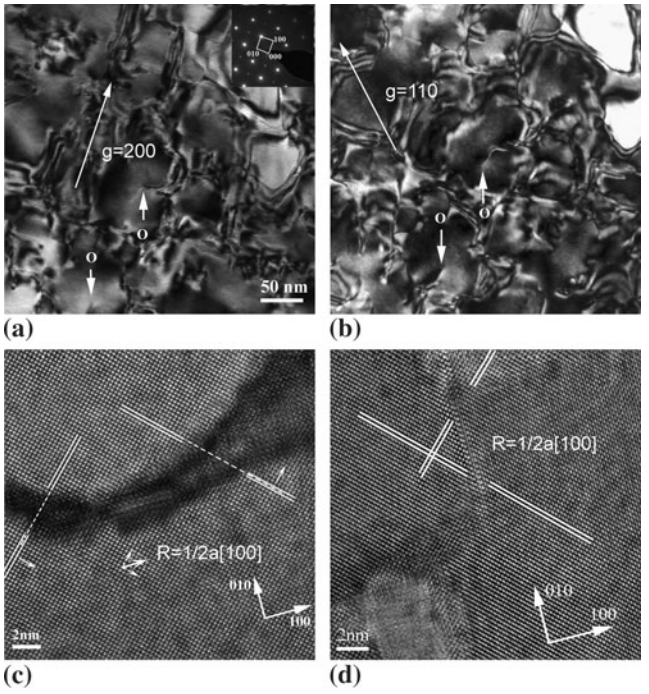


FIG. 3. (a) and (b) BF plane-view images of two-step-grown STO thin films, using g vectors 020 and 110, respectively. The dislocations inside the grains are indicated by "O". The inset of (a) shows the corresponding selected area diffraction pattern. (c) and (d) are the plane-view high-resolution images of two-step-grown STO thin films along [001].

stacking faults compared with single-step-grown STO films, where most interfacial dislocations are perfect-edge dislocations with Burgers vector $\boldsymbol{a}<100>$ and with only a few stacking faults.[12,13]

Figures 3(a) and 3(b) are plane-view BF images without substrates. The columnar-shaped grains are observed with a grain size of 50–100 nm, which is close to the distance between the stacking faults in Fig. 1. Some grain boundaries are curved, but most of them lie along the {100} planes. Inside the grains, there are only a few threading dislocations apparent in the film. However, the planar defects are not always closed; some of them are open and end at the dislocations. The corresponding SAED patterns proved that all these grains are epitaxially [001] orientated to the LAO substrate (not shown). The findings from the plane-view, bright-field images suggest that the contrasts in Figs. 1(b)–1(d) arise from the high density of the grain boundaries. To investigate the details of the boundary, we acquired high-resolution images in the plane view, as shown in Figs. 3(c) and 3(d). The former reveals an amorphous/void boundary separating two grains, whose width ranges from 0.6 to 6 nm. The upper part of the image displays a relative in-plane shift $\mathbf{R} = 1/2\boldsymbol{a}[100]$ to the lower part. Figure 3(d) shows another type of boundary from same sample, in which the central segment is a stacking fault with in-plane shift $\mathbf{R} = 1/2\boldsymbol{a}[100]$, whereas the other parts of boundary are voids. Altogether, we identified two kinds of grain boundaries/planar defects in

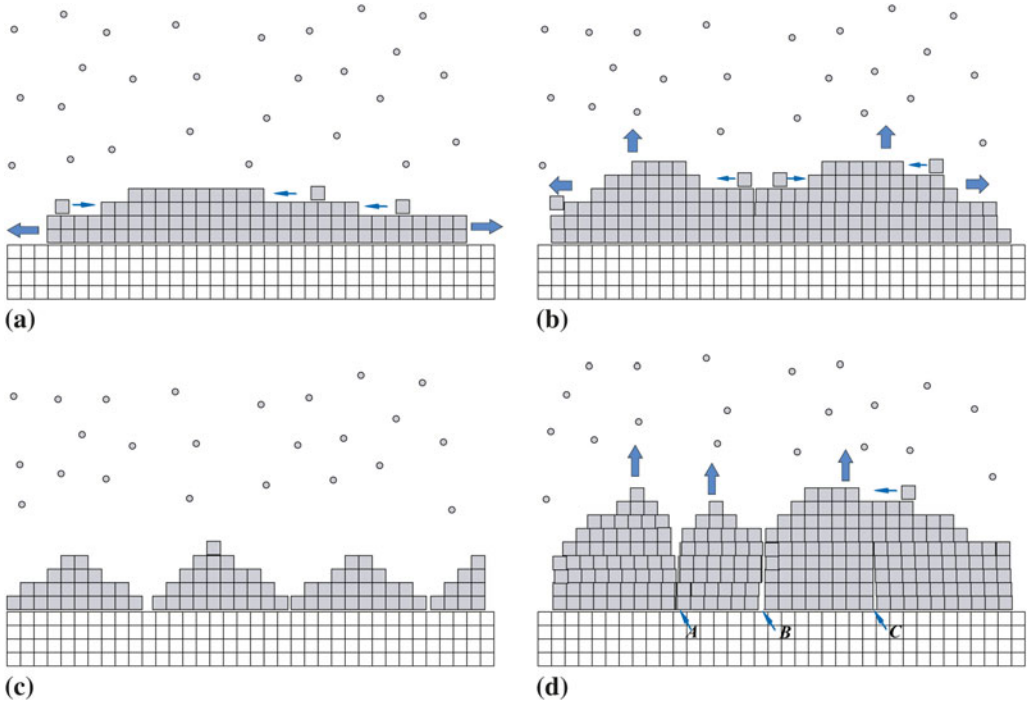


FIG. 4. Schematic models for the growth stages of STO films. (a) and (b) One-step-grown films: (a) completely coherent growth mode of the initial stage (layer-on-layer) and (b) layer-on-island growth after the thickness exceeds the critical thickness. (c) and (d) depict two-step-grown films: (c) after annealing the first layer and (d) 3D growth of the second layer. A, B, and C indicate the interface of grain boundaries.

https://doi.org/10.1557/jmr.2010.82 Published online by Cambridge University Press

terms of boundary width: a stacking fault grain boundary and a void/amorphous grain boundary. The former is a few atomic layers wide, whereas the latter is about several nanometers wide. Although similar void boundaries were reported in the (Ba, Sr)TiO_3/LAO system,[15] we cannot exclude the possibility of void formation during ion milling as we prepare our sample. On the other hand, amorphous-type planar defects were reported in $BaTiO_3$ deposited on $SrRuO_3/SrTiO_3$ systems; therein, amorphization was explained by the nonstoichiometric Ti/Ba ratios in the boundary.[16] However, we did not detect any compositional fluctuations in our thin films. In addition, as high-resolution imaging along the [001] zone axis did not distinguish any atomic shift along this orientation, we observed only a relative in-plane shift $\mathbf{R} = 1/2\boldsymbol{a}[100]$ or $1/2\boldsymbol{a}[010]$, which is a projection of $\mathbf{R} = 1/2\boldsymbol{a}[101]$ or $\mathbf{R} = 1/2\boldsymbol{a}[011]$ observed in Fig. 2.

Although partial dislocations and stacking faults with shift vectors along $1/2\boldsymbol{a}\langle 110\rangle$ were observed in one-step-grown STO film, their density was low; perfect dislocation half loops were the major defects.[12,13] However, the density of the planar defects (including stacking faults and grain boundaries) was much higher in the two-step-grown film than in one-step-grown films. The grain boundary should make a major contribution to relaxing the misfit strain because it has an in-plane component of shift and a high density.[9] The different features of the two-step-grown films and conventional ones can be understood from their growth modes; we compare them next.

For single-step-grown films, the growth mode is that of a 2D–3D island on a layer, as illustrated in Fig. 4(a). The initial STO monolayers grow coherently on the (001) LAO substrate via a layer-by-layer process. After the film's thickness reaches a critical value, the coherency of growth is partially broken by the appearance of dislocations that relax the misfit strain, and island nucleation occurs as illustrated in Fig. 4(b). Dislocation half-loops that form from the film's surface are seemingly the main source for misfit dislocations.[17,18]

For two-step thin films, the STO FL was deposited as an amorphous film on the LAO single crystal at room temperature. It was then crystallized during annealing at 750 °C. At this temperature, the STO crystal clusters nucleate inside the amorphous STO, and most probably also on the interface of LAO, with higher nucleation intensity than during conventional deposition at high temperature. Because of boundary mismatches or diffusion barriers, these clusters may not easily merge with each other, and consequently, a poly-grain layer is formed after annealing [Fig. 4(c)]. Our assumption is supported by the surface morphology of the FL, as evidenced by AFM. Figure 5(b) is an AFM image of 10-nm FL after annealing at 750 °C wherein STO grains are apparent; surface roughness slightly increases to about 0.8–0.9 nm, from average roughness of 0.3–0.4 nm of LAO substrate [Fig. 5(a)]. In addition, the size of these STO grain is about 40–75 nm, consistent with those shown in Fig. 3. At the following stage, the growth of STO follows a 3D mode, as illustrated in Fig. 4(d), because of the existence of the multigrain surface.[19,20] Grain boundaries are formed during the crystallization of FL, which are the major defects that relax the misfit strain. Growth is accompanied with the formation of stacking faults and amorphous- and void-like grain boundaries, depending on the surface mobility of the atoms relative to the deposition rate and by the substrate temperature relative to the melting temperature of the film.[11] During the deposition of the second layer, only a few misfit dislocations are generated by the half-loop mechanism. We note that the growth mode can be determined by the actual experimental conditions, such as oxygen partial pressure, growth temperature, deposition rate, and the surface condition of the substrate, and 3D growth have been reported for other systems.[16,19–23]

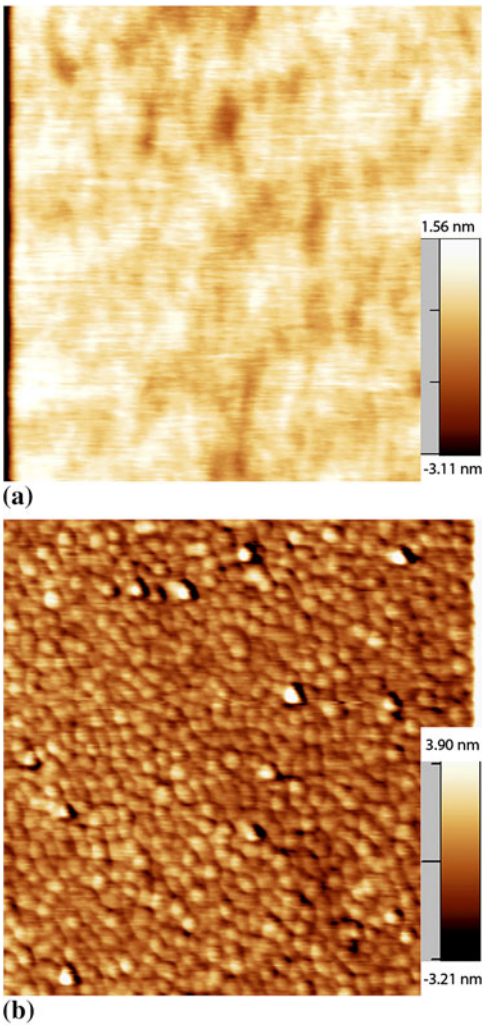


FIG. 5. Atomic force microscope images of (a) LAO substrate before deposition and (b) the first layer of STO after annealing at 750 °C. The scan size for both images was 1 × 1 μm^2.

https://doi.org/10.1557/jmr.2010.82 Published online by Cambridge University Press

IV. CONCLUSIONS

We investigated with TEM the microstructures of two-step-grown STO thin films deposited on LAO using PLD. In comparison to the perfect misfit dislocations and the threading dislocations found in single-step-grown films, the major defects in the two-step-grown films were partial misfit dislocations and planar defects. The annealed FL of the latter has a multigrain nature. Thereafter, the second STO layer grows on this multigrain template via 3D island growth. We suggest that grain boundaries and interfacial dislocations primarily are responsible for the relaxation of misfit strain.

ACKNOWLEDGMENTS

This work was supported in part by the Swiss National Science Foundation. N. Jiang gratefully acknowledges the financial support from National Science Foundation (NSF), DMR-0603993.

REFERENCES

1. O.G. Vendik, E.K. Hollman, A.B. Kozyrev, and A.M. Prudan: Ferroelectric tuning of planar and bulk microwave devices. *J. Supercond.* **12**, 325 (1999).
2. A.K. Tagantsev, V.O. Sherman, K.F. Astafiev, J. Venkatesh, and N. Setter: Ferroelectric materials for microwave tunable applications. *J. Electroceram.* **11**, 5 (2003).
3. N.A. Pertsev, A.K. Tagantsev, and N. Setter: Phase transitions and strain-induced ferroelectricity in $SrTiO_3$ epitaxial thin films. *Phys. Rev. B* **61**, R825 (2000).
4. C.L. Canedy, H. Li, S.P. Alpay, L. Salamanca-Rica, A.L. Roytburd, and R. Ramesh: Dielectric properties in heteroepitaxial $Ba_{0.6}Sr_{0.4}TiO_3$ thin films: Effect of internal stresses and dislocation-type defects. *Appl. Phys. Lett.* **77**, 1695 (2000).
5. H. Li, A.L. Roytburd, S.P. Alpay, T.D. Tran, L. Salamanca-Riba, and R. Ramesh: Dependence of dielectric properties on internal stresses in epitaxial barium strontium titanate thin films. *Appl. Phys. Lett.* **78**, 2354 (2001).
6. J.H. Haeni, P. Irvin, W. Chang, R. Uecker, P. Reiche, Y.L. Li, S. Choudhury, W. Tian, M.E. Hawley, B. Craigo, A.K. Tagantsev, X.Q. Pan, S.K. Streiffer, L.Q. Chen, S.W. Kirchoefer, J. Levy, and D.G. Schlom: Room-temperature ferroelectricity in strained $SrTiO_3$. *Nature* **430**, 758 (2004).
7. B.H. Park, E.J. Peterson, Q.X. Jia, J. Lee, X. Zeng, W. Si, and X.X. Xi: Effects of very thin strain layers on dielectric properties of epitaxial $Ba_{0.6}Sr_{0.4}TiO_3$ films. *Appl. Phys. Lett.* **78**, 533 (2001).
8. T. Yamada, K.F. Astafiev, V. Sherman, A.K. Tagantsev, P. Muralt, and N. Setter: Strain relaxation of epitaxial $SrTiO_3$ thin films on $LaAlO_3$ by two-step growth technique. *Appl. Phys. Lett.* **86**, 142904 (2005).
9. T. Yamada, K.F. Astafiev, V. Sherman, A.K. Tagantsev, D. Su, P. Muralt, and N. Setter: Structural and dielectric properties of strain-controlled epitaxial $SrTiO_3$ thin films by two-step growth technique. *J. Appl. Phys.* **98**, 54105 (2005).
10. T. Yamada, V. Sherman, D. Su, A.K. Tagantsev, P. Muralt, and N. Setter: Growth process approaches for improved properties of tunable ferroelectric thin films. *J. Eur. Ceram. Soc.* **27**, 3753 (2007).
11. L.B. Freund and S. Suresh: *Thin Film Materials: Stress, Defect Formation and Surface Evolution* (Cambridge Press, 2004), pp. 16.
12. D. Su, T. Yamada, V. Sherman, A.K. Tagantsev, P. Muralt, and N. Setter: Annealing effect on dislocations in $SrTiO_3/LaAlO_3$ heterostructures. *J. Appl. Phys.* **101**, 64102 (2007).
13. Y.L. Qin, C.L. Jia, K. Urban, J.H. Hao, and X.X. Xi: Dislocations in $SrTiO_3$ thin films grown on $LaAlO_3$ substrates. *J. Mater. Res.* **17**, 3117 (2002).
14. C.J. Lu: Type of dissociated misfit dislocation in perovskite films on $LaAlO_3$. *Appl. Phys. Lett.* **85**, 2768 (2004).
15. X. Zhu, H.L.-W. Chan, K.-H. Wong, and D. Hesse: Microstructure of compositionally graded $(Ba_{1-x}Sr_x)TiO_3$ thin films epitaxially grown on $La_{0.5}Sr_{0.5}CoO_3$-covered (100) $LaAlO_3$ substrates by pulsed laser deposition. *J. Appl. Phys.* **97**, 093503 (2005).
16. J.Q. He, E. Vasco, R. Dittmann, and R.H. Wang: Growth dynamics and strain-relaxation mechanisms in $BaTiO_3$ pulsed laser deposited on $SrRuO_3/SrTiO_3$. *Phys. Rev. B* **73**, 125413 (2006).
17. T. Suzuki, Y. Nishi, and M. Fujimoto: Analysis of misfit relaxation in heteroepitaxial $BaTiO_3$ thin films. *Philos. Mag. A* **79**, 2461 (1999).
18. H.P. Sun, X.Q. Pan, J.H. Haeni, and D.G. Schlom: Structural evolution of dislocation half-loops in epitaxial $BaTiO_3$ thin films during high-temperature annealing. *Appl. Phys. Lett.* **85**, 1967 (2004).
19. F. Sanchez, G. Herranz, I.C. Infante, J. Fontcuberta, M.V. Garcia-Cuenca, C. Ferrater, and M. Varela: Critical effects of substrate terraces and steps morphology on the growth mode of epitaxial $SrRuO_3$ films. *Appl. Phys. Lett.* **85**, 1981 (2004).
20. W.C. Goh, S.Y. Xu, S.J. Wang, and C.K. Ong: Microstructure and growth mode at early growth stage of laser-ablated epitaxial Pb $(Zr_{0.52}Ti_{0.48})O_3$ films on a $SrTiO_3$ substrate. *J. Appl. Phys.* **89**, 4497 (2001).
21. J.C. Jiang and X.Q. Pan: Microstructure and growth mechanism of epitaxial $SrRuO_3$ thin films on (001) $LaAlO_3$ substrates. *J. Appl. Phys.* **89**, 6365 (2001).
22. A. Visinoiu, M. Alexe, H.N. Lee, D.N. Zakharov, A. Pignolet, D. Hesse, and U. Gösele: Initial growth stages of epitaxial $BaTiO_3$ films on vicinal $SrTiO_3$ (001) substrate surfaces. *J. Appl. Phys.* **91**, 10157 (2002).
23. J. Shin, S.V. Kalinin, A.Y. Borisevich, E.W. Plummer, and A.P. Baddorf: Layer-by-layer and pseudo-two-dimensional growth modes for heteroepitaxial $BaTiO_3$ films by exploiting kinetic limitations. *Appl. Phys. Lett.* **91**, 202901 (2007).

https://doi.org/10.1557/jmr.2010.82 Published online by Cambridge University Press